Characterization of Welding Fume from SMAW Electrodes — Part I

Size and mass distributions, fume generation rates, and chemistry are compared for three SMAW electrodes

BY J. W. SOWARDS, J. C. LIPPOLD, D. W. DICKINSON, AND A. J. RAMIREZ

ABSTRACT. An electrical low pressure impactor (ELPI) was used to collect welding fume from E6010 and E308-16 electrodes at two heat input levels, and E7018 electrodes at a nominal heat input level. This paper describes the collection procedures and presents data on the fume generation rates (FGR), particle number and mass distributions as a function of size, and identifies compounds present in the bulk fume. Part II of this paper describes the detailed characterization of this fume conducted using transmission and scanning electron microscopy, and a surface-sensitive analysis technique known as X-ray photoelectron spectroscopy.

Using the ELPI, the fume is separated by particle size in 13 size ranges from 0.03 to 10 micrometers. Size and mass distributions were determined over these size ranges for the three consumables using this technique. Fume was also collected using a modified AWS F1.2:1999 bulk collection technique to determine fume generation rates and provide samples for bulk X-ray diffraction (XRD) studies. X-ray diffraction revealed that the predominant phase in fume generated by all electrodes was a Fe_3O_4 compound (magnetite) with some substitution of Mn and Si for Fe in the magnetite structure. Fume generation rates were highest for E6010 followed by E7018 and E308-16, respectively. Varying heat input changed fume generation rates but did not affect the chemical nature of the fume, nor alter the size and mass distributions to any great extent. Particle size distributions of all three electrodes reached peak concentrations in the fine (0.1–2.5 μm) particle size regions.

Introduction

Fume generated by the shielded metal arc welding (SMAW) process may be a cause for concern due to possible health problems experienced by individuals in the welding industry after long-term exposure. Welding fume particles may cause metal fume fever, and perhaps more importantly, manganese- or chromium-related poisoning after inhalation and ingestion into the human body. For example, it has been proposed that long term, low concentration doses of Mn are linked to nervous system disorders (Ref. 1). Studies have also shown that welders working with stainless steels who have had cases of lung cancer may be due to possible hexavalent chromium exposure, although there has been no direct evidence linking the cancer to welding fume exposure (Ref. 2). Occupational exposure limits (OEL), which are revised quite regularly (Ref. 3), determine the amount of these compounds and elements that may be ingested without becoming harmful to human tissues. Though epidemiological reactions to the different compounds present in welding fume are important, they are beyond the scope of this study, which was designed to characterize the fume particles produced by metal joining processes.

An aerosol consisting of fume and spatter is produced during welding with SMAW electrodes. Previous studies have shown that SMAW fume consists of an assortment of metals, oxides, and other compounds, which form from evaporation of elements in the arc and fluxes covering the electrode (Refs. 4–6). The fume particles generally vary over a wide range of sizes, thus it becomes important to consider fume particles in each size range as opposed to bulk composition alone. Relationships between particle size and composition have also been found (Refs. 5, 7). Number and mass distributions of welding fumes have been measured with a variety of techniques including cascade impactors, scanning mobility particle sizers, and optical particle counters (Refs. 5, 7–9). These distributions have typically shown that fume particles are present in a broad range of sizes but are generally present in higher concentrations of small particle sizes and higher masses of the larger particle sizes.

Fume formation is of great interest in order to understand the varying morphologies and compositions of bulk fume. The effect of aerosol physics on welding fume formation have been described in detail by Zimmer et al. (Refs. 9, 10). Jenkins has provided a thorough summary of formation mechanisms and corresponding size ranges that govern welding fume particle formation (Ref. 7). The three mechanisms and approximate formation ranges are nucleation (< 100 nm), accumulation (100 nm–1 μm), and the coarse range (> 1 μm). The degree of particle growth in the nucleation range is primarily controlled by the amount of supercooling following particle nucleation. Accumulation describes particle growth by collision with other particles from diffusion and impaction. As particles continue to collide with one another they may also form agglomerates, which may adhere due to a number of mechanisms. These include 1) contact of multiple particles still in the liquid state, 2) sintering, and 3) electrostatic and Van der Waals forces (Ref. 11).

Agglomerate sizes may be large compared to individual particles, yet their aerodynamic diameters can still be quite small. An aerodynamic diameter is the diameter of a unit density sphere with the same particle mass and particle mobility as the particle in question (Refs. 11, 12). Aerodynamic diameter can be quite low for open structured agglomerates, compared to spherical particles (Ref. 13). Coarse fume particles are formed by mechanical means such as ejection of spatter

KEYWORDS

Electrical Low Pressure Impactor (ELPI)
Shielded Metal Arc Welding (SMAW)
Fume Generation Rates (FGR)
X-Ray Diffraction (XRD)
E6010, E308-16, and E7018

J. W. SOWARDS, J. C. LIPPOLD, and D. W. DICKINSON are with the Welding & Joining Metallurgy Group, The Ohio State University, Columbus, Ohio. A. J. RAMIREZ is with the Brazilian Synchrotron Light Laboratory, Campinas, SP, Brazil.

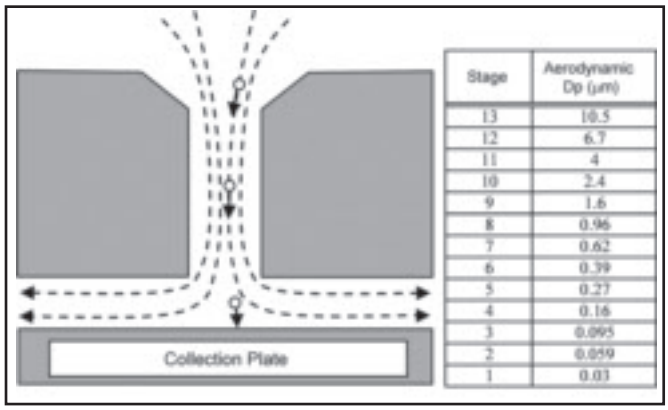

Stage	Aerodynamic Dp (μm)
13	10.5
12	6.7
11	4
10	2.4
9	1.6
8	0.96
7	0.62
6	0.39
5	0.27
4	0.16
3	0.095
2	0.059
1	0.03

Fig. 1 — Principle of particle impaction and aerodynamic cutoff size ranges of each ELPI stage (Ref. 24).

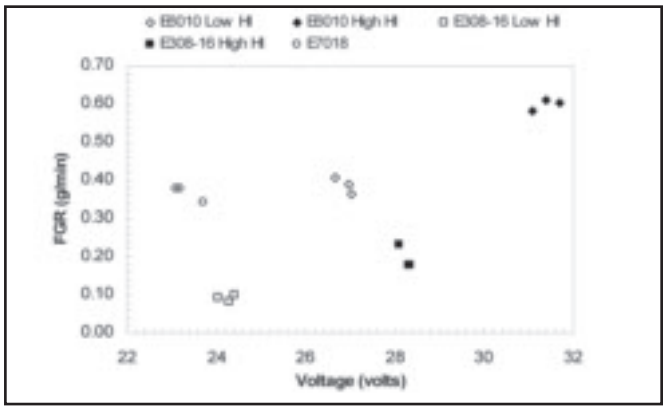

Fig. 2 — Effect of voltage on fume generation rates of E6010, E308-16, and E7018.

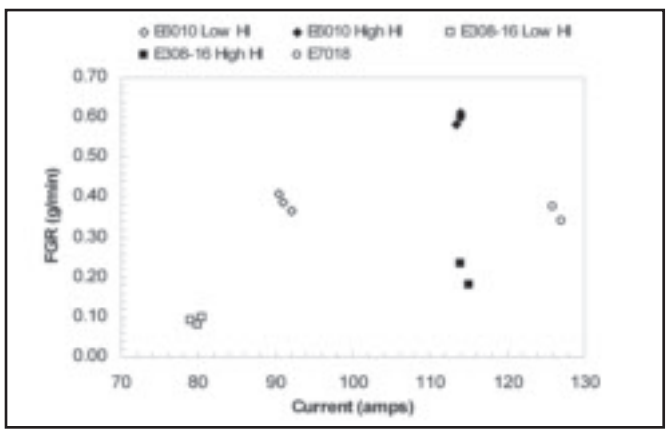

Fig. 3 — Effect of current on fume generation rates of E6010, E308-16, and E7018.

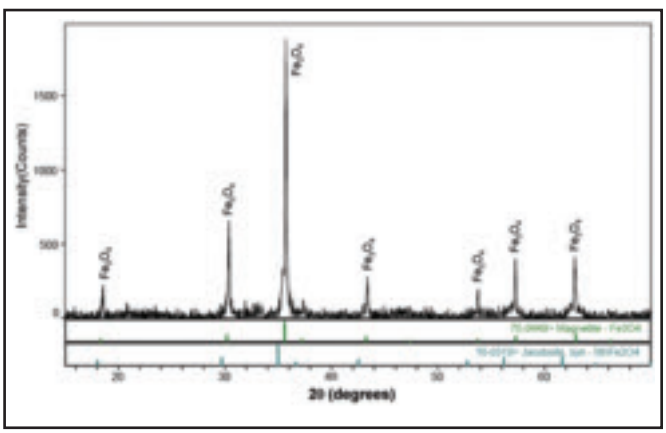

Fig. 4 — X-ray diffraction spectrum obtained from E6010 electrode (60-s collection, 16.3 kJ/in. heat input).

from the arc or molten weld pool. These formation factors must be considered when analyzing composition and particle size distributions.

Fume generation rates (FGR) of SMAW electrodes are second only to flux cored arc welding (FCAW) processes among the various welding processes that are used commercially (Ref. 14). Fume generation is a function of different formation steps and competing mechanisms (Refs. 7, 10). The dynamics of aerosol nucleation and fume formation are thoroughly described elsewhere (Refs. 15, 16). The various elements and compounds within the welding consumable and base material are vaporized as a result of the intense heat produced by the welding arc. A general sequence of welding fume formation is as follows after vaporization: 1) the aerosol particles will homogonously nucleate from the supersaturated vapor; 2) then they will grow by condensation and/or coagulation; 3) possibly develop a core-shell structure by condensation due to varying vapor pressure of different species, or due to liquid phase separation; 4) form an oxide shell around the metallic core due to the exposure of the aerosol particle to oxygen-rich atmosphere; 5) fully react with oxygen to form metal-oxides; and 6) coagulate to form aerosol particle agglomerates. If flux is used, as is the case with SMAW and FCAW electrodes, then the fume particle will be exposed to vapor formed from the vaporized flux elements resulting in condensation of additional elements on preexisting particles.

Condensation temperature variations between compounds such as Fe_3O_4 and SiO_2 in aerosols have been shown to contribute to regions of compositional variation in the individual particles, leading to a "core-shell" morphology (Ref. 17). These different formation mechanisms will result in a large size-range of particles during shielded metal arc welding, ranging

Table 1 — Welding Conditions and Calculated Heat Input

Welding Parameter	E6010 Low Heat Input	E6010 High Heat Input	E308-16 Low Heat Input	E308-16 High Heat Input	E7018 Nominal Heat Input
Current, Amps	93	115	81	115	126
Voltage, Volts	27.1	30.8	24	24	23.8
Travel Speed, in./min (mm/s)	9.6 (4.1)	11.1 (4.7)	10.5 (4.4)	10.5 (4.4)	10.75 (4.6)
Heat Input, kJ/in. (kJ/mm)	15.8 (0.62)	19.1 (0.75)	11.1 (0.44)	17.3 (0.68)	16.8 (0.66)
Electrode Diameter, in. (mm)	⅛ (3.2)	⅛ (3.2)	⅛ (3.2)	⅛ (3.2)	⅛ (3.2)
Coating Type	High Cellulose Sodium		Neutral Basic		Basic, Low Hydrogen

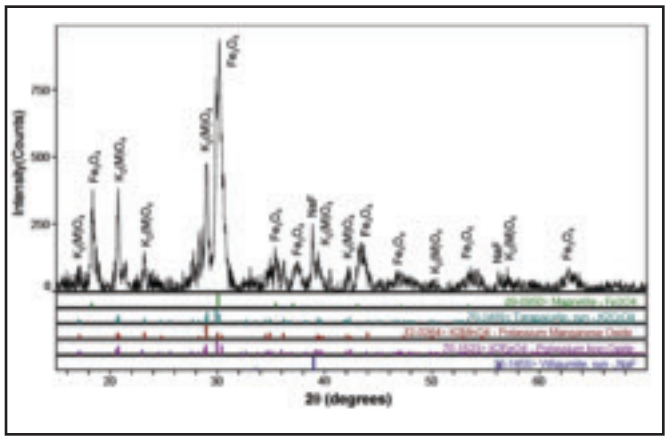

Fig. 5 — X-ray diffraction spectrum obtained from E308-16 electrode (135-s collection, 21.2 kJ/in. heat input).

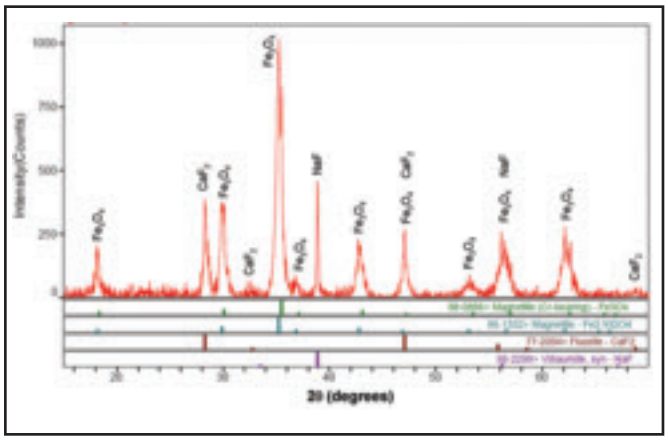

Fig. 6 — X-ray diffraction spectrum obtained from E7018 electrode (60-s collection, 14.5 kJ/in. heat input).

from ultrafine (<0.1 μm) to fine (0.l–2.5 μm) to coarse (>2.5 μm) sizes (Ref. 18). The fine and ultrafine size ranges have been suggested to be the main concern with respect to possible health problems, since they are more likely to be deposited in the lungs. Techniques, such as those described here, to characterize the nature of welding fume as a function of size distributions are required to fully understand the health-related impact of welding fume.

A fume collection system and procedure has been developed and was used to test the three electrodes in this study as well as a number of other consumable/process combinations. This testing includes collection of fume and measurement of FGR using an AWS-type collection system, coupled with smaller filter pore sizes than those recommended by the F1.2:1999 standard (Ref. 19). A critical component of these studies is the fume collection with an electrical low pressure impactor (ELPI). The ELPI is capable of separating particles by aerodynamic diameter and monitoring size distributions in real time. This is accomplished through various principles including particle charging, inertial classification, and electrical detection of the particles using electrometers (Ref. 20). Fume is drawn into the ELPI by means of a vacuum pump, and is passed through a particle charger before being separated in the impactor. The impactor has multiple stages, which size particles according to their aerodynamic diameter in the range of 0.03–10 μm. A given stage will trap particles if they are unable to make the sharp turn required, due to their inertia, to reach the next stage. This principle of particle impaction along with the particle size trapped by each stage is shown in Fig. 1. Each stage has the capability to detect the charge on the incoming particles via electrometers thus allowing for real-time monitoring by a PC data acquisition system. Weight analyses are commonly used in fume studies but the large particles, even if they are low in concentration, may dominate a percent weight analysis (Ref. 21). Therefore, a considerable advantage to using an ELPI system is its ability to retrieve a particle number distribution for a fume collection in addition to measuring mass collected on each stage of the system.

Table 2 — Fume Generation Rates

Electrode	E6010	E6010	E308-16	E308-16	E7018
Heat input (kJ/in.)	15.8	19.1	11.1	17.3	16.8
Average FGR (g/min)	0.387	0.598	0.091	0.198	0.365

Table 3 — Statistical Analyses Results for Number and Mass Distributions Presented in Figs. 6 and 7. Diameter Values are Reported in Nanometers.

	E6010 Low HI	E6010 High HI	E308-16 Low HI	E308-16 High HI	E7018
			number distributions		
d_g	102.4	128.7	206.2	252.9	105.1
σ_g	1.18	1.18	1.18	1.15	1.25
67%	87.1	108.9	175.0	220.4	84.2
	120.4	152.1	243.0	290.3	131.2
95%	43.6	54.5	87.5	110.2	42.1
	240.8	304.2	486.0	580.6	262.5
			mass distributions		
d_g	592.0	661.5	624.8	556.7	746.5
σ_g	1.13	1.17	1.11	1.11	1.32
67%	524.9	563.6	561.4	501.1	566.1
	667.7	776.5	695.3	618.5	984.5
95%	262.4	281.8	280.7	250.5	283.0
	1335.4	1553.0	1390.6	1237.0	1968.9

Procedure

A detailed procedure developed by Sowards et. al was followed for the analysis of welding fume from SMAW electrodes (Ref. 22). A36 steel was used as a base material for E6010 and E7018 electrodes, and Type 304L stainless steel was used as a base material for the E308-16 electrode. All welding procedures used were in accordance with the consumable manufacturer recommendations, i.e., operating current, voltage, work angle, and low-hydrogen electrode control (E7018,

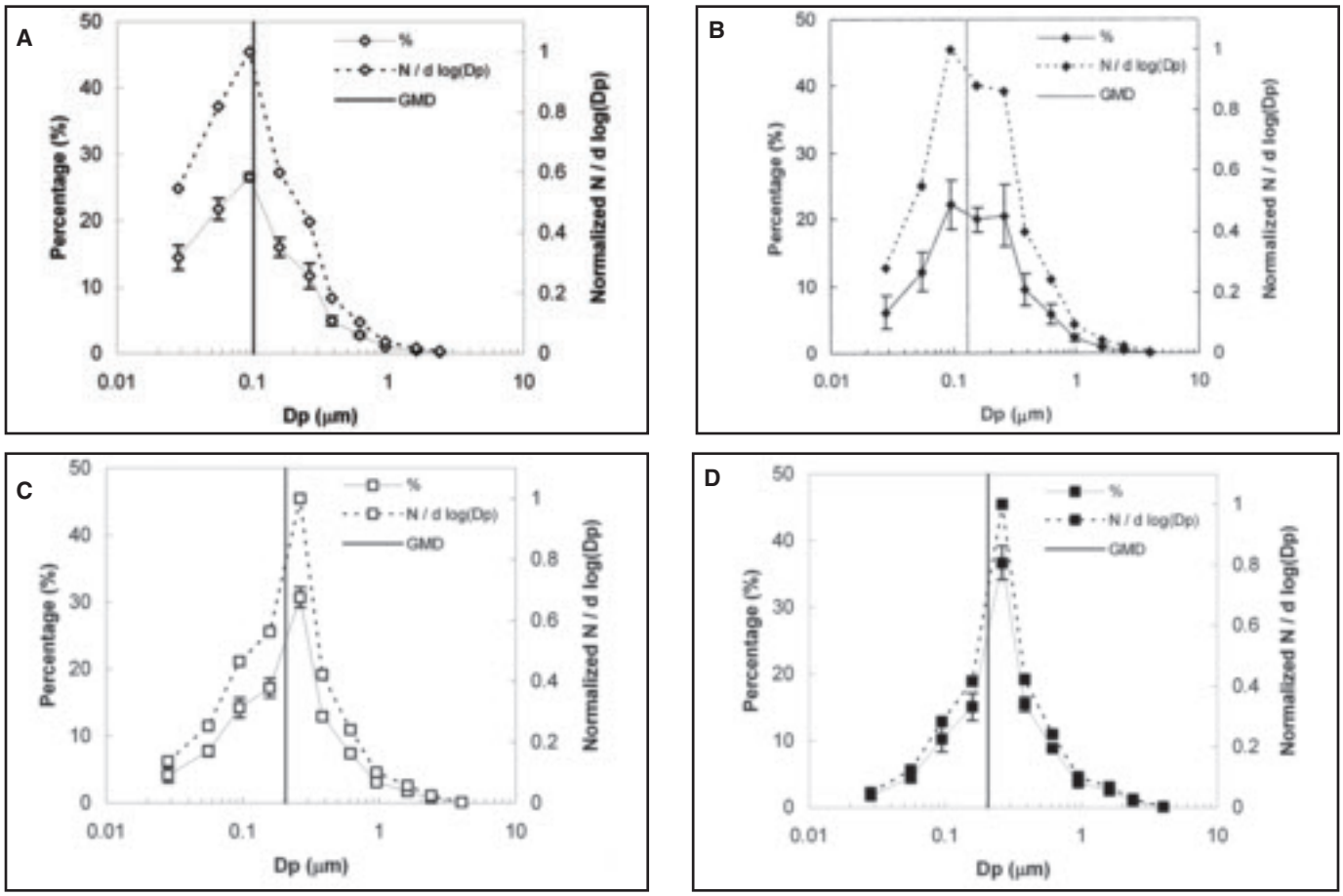

Fig. 7 — Particle number distributions as a function of particle diameter for the following: A — E6010 low heat input; B — E6010 high heat input; C — E308-16 low heat input; D — E308-16 high heat input; E — E7018 nominal heat input. Vertical lines correspond to geometric mean diameter (GMD) of distributions.

E308-16). All welds were performed in the flat position, and the base material was moved relative to the electrode using a linear positioner for ELPI collections and rotary positioner for fume hood collections. An arc voltage controller (AVC) was used in conjunction with a linear positioner to feed the covered electrodes while maintaining a constant arc voltage, thus maintaining repeatability of heat input. All welding parameters were monitored and recorded during testing. Averages of the parameters were used to calculate heat input as shown in Table 1. Heat input is a commonly used parameter for specifying a welding procedure, therefore two levels were used. It was not a goal of this study to examine the effect of voltage and current on fume formation.

Fume was collected in a sequence of several trials. The first consisted of using the fume hood to measure fume generation rates and collect bulk samples for X-ray diffraction (XRD) analysis. High flow-rate glass fiber filters with a pore size of 0.3 μm and an efficiency of 99.98% were used for these collections. The filters were non-hygroscopic so moisture in the atmosphere had negligible effect on filter weights. A digital manometer with PC control was used to record pressure drop across the filter during all fume hood collection. The pressure drop provides insight into filter performance and indicates when the filters become saturated with fume. Due to limited physical space in the fume hood chamber, a rotary positioner with DC stepper control was used to provide base metal travel instead of the linear positioner used in ELPI collections.

After FGR were measured, the ELPI was used to collect fume for particle number and mass distributions. Particle number distributions were recorded in real time by the ELPI. Mass distributions were obtained by weighing aluminum collection substrates placed on each stage of the ELPI. Following a collection run, the substrate on each stage was reweighed to find the fume mass deposited during testing. Substrate weight was measured to an accuracy of 10^{-5} grams with an analytical balance.

Results and Discussion

Fume Generation Rate

The fume generation results for E6010, E7018, and E308-16 electrodes using the modified fume collection hood are presented in Table 2. These FGR values represent an average of three collections for

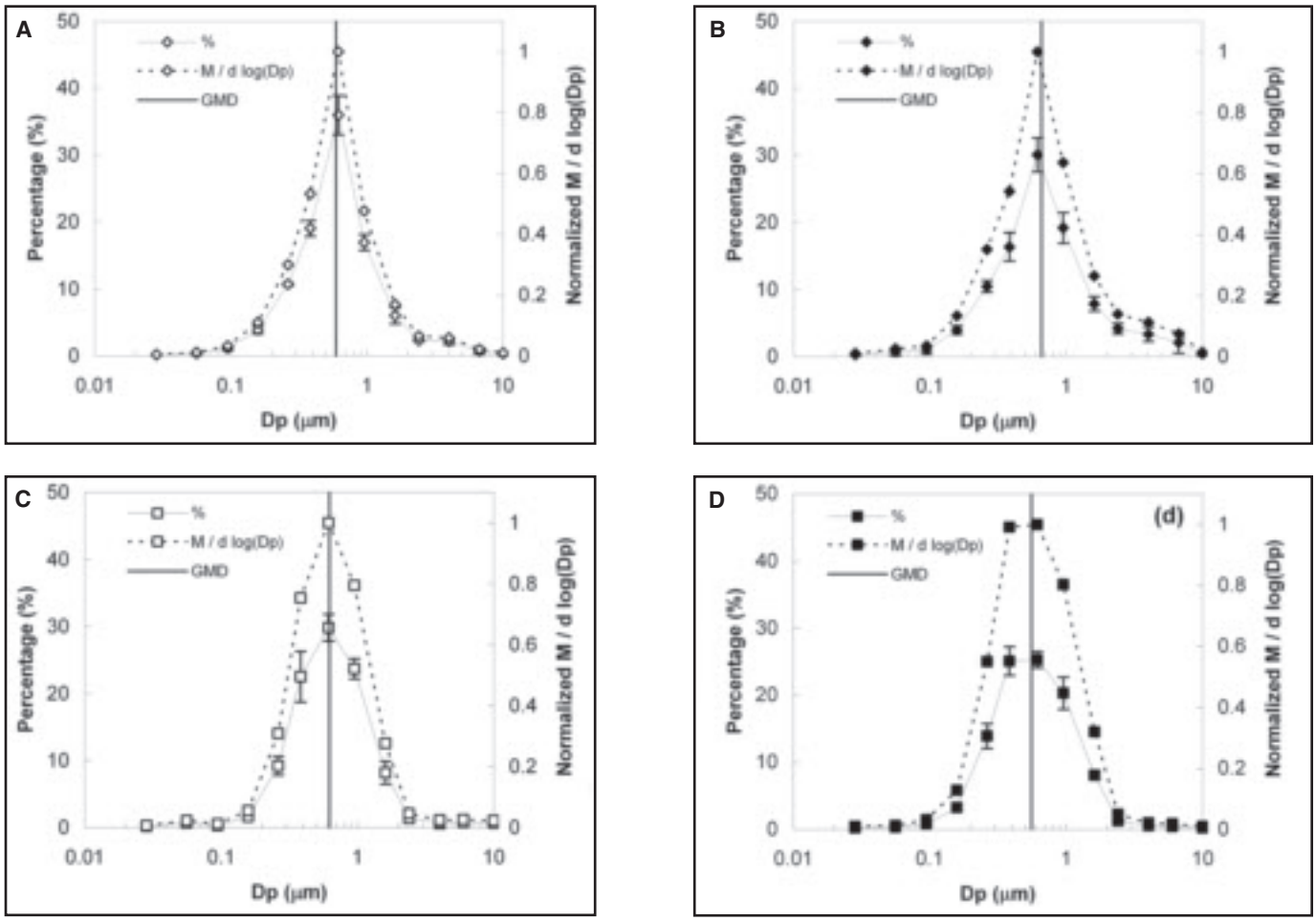

Fig. 8 — Particle mass distributions as a function of particle diameter for the following: A — E6010 low heat input; B — E6010 high heat input; C — E308-16 low heat input; D — E308-16 high heat input; E — E7018 nominal heat input. Vertical lines correspond to geometric mean diameter (GMD) of distributions.

each electrode. The total fume generated for the E7018 was slightly less than the E6010 electrode at low heat input suggesting E6010 has the highest relative FGR. E308-16 generated less than 25% of the fume of both mild steel electrode fumes at the lower heat input level. Qualitative visual examination revealed that the E308-16 welds had a much thicker slag coating, which likely equates to a larger percentage of the flux coating ending up as slag instead of fume as compared with the other electrodes. Also, melting and vaporization rates of mild and stainless steels are considerably different because of differences in thermal conductivity as compared to mild steels. Effects of voltage and current on FGR are shown in Figs. 2 and 3, respectively. Each point represents the average current and voltage recorded for a given electrode over the duration of the weld. Three welds were made at each heat input level. For both E6010 and E308-16, an increase in fume generation was noted with increasing current and voltage (i.e., between the two levels of heat input).

X-Ray Diffraction Results

X-ray diffraction was performed on bulk fume filters from each of the electrodes to identify metallic species or compounds present in the fume. The samples contained the full particle size range as described in the procedure section. Fume was removed from the bulk filter and pressed onto zero background holders before the diffraction experiments took place, providing a better peak to background ratio than the fume filter itself. Figure 4 shows the results for the E6010 electrode after a 60-s collection with the fume hood. The peaks show a strong correlation to a magnetite (Fe_3O_4) type structure. However, slight peak shifts were present, suggesting the other elements (Mn and Si) are substituting for Fe and shifting the 2θ values.

X-ray diffraction results for E308-16 transferred fume are shown in Fig. 5. These peaks show the presence of magnetite (Fe_3O_4) and a potassium-rich oxide (K_2MO_4). The M in the formula represents Fe, Mn, Ni, or Cr. Based on the spectrum, it is not possible to separate the in-

dividual compounds for these peaks. Therefore, M should be considered as a mixture of the four metals, although TEM analysis showed that the predominant element is Fe. A weak match for NaF was also observed in the E308-16 spectrum. The XRD spectrum for the E7018 fume (Fig. 6) has strong peaks for Fe_3O_4, CaF_2, and NaF. Once again, slight 2θ shifts were observed for the magnetite peaks, which were most likely caused by a Mn and Si substitution for Fe.

Number and Mass Distributions

The ELPI was used to measure both size and mass distributions using the techniques described previously. The number distribution, measured by the ELPI as a function of the aerodynamic diameter, was determined for two heat input conditions of E6010 and E308-16 and a single heat input of E7018. Resulting distributions are presented in Fig. 7 where the normalized number of particles (dN/d log(Dp)) is plotted vs. log of particle diameter, Dp. The mass distributions of the same collections are presented in Fig. 8 where normalized particle mass (dM/d log(Dp)) is plotted vs. log of particle diameter. It is convenient to plot aerosol distributions vs. the log of particle diameter to compress the region containing coarse particles and enlarge the fine and ultrafine regions since these are of greatest interest. Percentage of particle size and mass for each ELPI stage are also included in Figs. 7 and 8. Error bars indicate one standard deviation (for percentage scale) of the average of three collections performed for each condition. Geometric mean diameters are represented by the vertical dashed line shown on each distribution. Statistical analyses may be performed on log-normal distributions of aerosols to obtain a geometric mean diameter and variance of particle size. Results of these statistical analyses are displayed in Table 3.

E6010 — Distributions

Comparing the particle number distributions between the two different heat inputs of E6010 fume (Fig. 7A and B) shows good consistency. Approximately 95% of particles are less than 0.3 μm in diameter, making the bulk of the size distributions for both heat inputs lie in the particle nucleation and accumulation size ranges as described elsewhere (Ref. 7). More than 70% of the fume mass lies in the accumulation range (particles below 1 μm in diameter). The mass of particles below 0.1 μm is very small, representing less than 2% of the total fume mass. Geometric mean diameters of the number distributions were both at the transition between the nucleation and accumulation ranges, suggesting these are the dominant fume formation mechanisms, though there is some speculation in distinction between the two regions (Ref. 9). E6010 distributions change only slightly with heat input as shown by the similar results in statistical methods. The number distribution for the high heat input welds is slightly skewed to larger average particle sizes relative to the low heat input collections. Both heat input levels had the highest percentage based on total weight at approximately 0.6 μm average aerodynamic diameter.

E308-16 — Distributions

The average number percentage for the E308-16 electrode as a function of the aerodynamic diameter as measured from the ELPI stages for both heat inputs are presented in Fig. 7C and D and mass distributions for both heat input conditions are shown in Fig. 8C and D. Similar to what was observed for the E6010 electrodes, there was little change in size distribution between the low and high heat input welds. The number distribution shifts to larger particle sizes, and mass distribution decreases slightly in diameter for the higher heat input. Particles in the size range of approximately 0.2–0.3 μm were predominant, accounting more than 60% of the total number of particles. Comparing the E6010 to the E308-16, the particle size distribution is biased toward the large size particles in the E308-16 fume. This may be related to the degree of supercooling between the two materials or because of different nucleation rates. The E308-16 fume contains Ni and Cr, which have lower thermal conductivities than the strictly Fe-based particles found in E6010 fume. Since these particles may have slower cooling than the E6010 particles, they could possibly have more time to grow by diffusion after colliding with more particles. The mass distribution between the two heat inputs is also consistent. Mass distribution was spread over a wider particle size range than the E6010. Once again, the mass of particles below 0.1 μm is very small, accounting for about 1.5% of the total fume mass.

E7018 — Distributions

Average number and mass distributions for E7018 at a nominal heat input are presented in Figs. 7E and 8E, respectively. The number distribution of E7018 is shifted toward the small aerodynamic diameters of the ELPI size range as compared with number distributions of E6010 and E308-16, which both exhibited distributions with the majority of the particles falling in the 0.1–0.2 μm size range. The mass distribution of E7018 peaks at approximately 0.6 μm average diameter with a geometric mean diameter of 0.75 μm. The mean diameter is increased since higher masses were measured on the larger stages of the ELPI. The size and mass distributions appeared multimodal. The size distribution had a mode in the nucleation and accumulation range. The mass distribution had an additional mode in the coarse range, which may be associated with spatter formation (Ref. 10).

Summary of Number and Mass Distribution Results

Clearly the number distributions for the three electrodes are biased toward smaller diameter particles as compared with mass distributions. However, the mass of these small particles is insignificant in comparison with mass of the particle sizes where mass distribution peaks (0.6–0.75 μm). Some speculation exists as to which size range of fume particles, whether it is the fine or ultrafine regions, are most damaging when inhaled by welding personnel (Ref. 18). It is generally accepted that respirable particles are those that are less than 10 μm in size. Agglomerates of various sizes were present on all stages of the ELPI collections for each of the electrodes tested as observed by characterization techniques discussed in Part II of this paper. Equivalent aerodynamic diameters of agglomerates must be considered when analyzing data from the ELPI, since it only provides an average behavior of each stage cut-off size. Agglomerated particles may have a large physical size compared to their aerodynamic diameter. Thus, larger-sized agglomerates may be collected on the lower stages of the impactor. For all three electrodes, a high percentage of the fume particles on the lower stages were agglomerates, while the upper stages contained a higher fraction of spherical particles. The higher fraction of isolated spherical particles on upper stages may be explained by the fact that spatter is the dominant fume formation mode at the larger size scales as opposed to particle accumulation (Refs. 7, 10).

As this occurs, seemingly large agglomerates are counted on the lower stages because their aerodynamic diameter is actually small. Models of the human oral-pharyngeal cavities suggest that these agglomerates that are held together by Van der Waals forces may disperse back into individual particles if the flow rate is substantially large as in human lung models (30–200 L/min) (Ref. 23). The ELPI used for this study was only operated at a flow rate of 10 L/min, which is not adequate to break these loosely attractive forces. However, many of these agglomerates are held together by forces other than Van der Waals bonding suggesting agglomerate disassociation will likely not

occur for those other types. Even with agglomeration effects, the ELPI distribution, based on aerodynamic diameter, is a good representation of the respirable ranges of these particles.

The information made available in this manuscript provides insight on fume formation and size distribution of SMA welding fumes. This information along with the characterization of SMA fume in Part II of this study may be useful for future welding consumable development, since consumable composition affects the nature of the fume it generates.

Conclusions

1. Fume generation rate is dependent on heat input and varied among the electrodes evaluated, being highest for E6010 electrode, followed by E7018 and E308-16.

2. X-ray diffraction of E6010 and E7018 bulk fume samples revealed that the primary phase present was Fe_3O_4 (magnetite). Slight peak shifts suggested that Mn and Si probably substituted for Fe in the Fe_3O_4-type structure. The E7018 fume had additional peaks for NaF and CaF_2.

3. X-ray diffraction of the E308-16 fume also showed strong peaks for Fe_3O_4 and had additional peaks for K_2MO_4 (M accounts for Fe, Mn, Ni, Cr) and NaF.

4. Particle number distributions determined with the ELPI for E6010 and E7018 showed that 95% of the fume particles generated during welding were smaller than 0.3 μm. For E308-16, 95% of the fume consisted of particles less than approximately 0.6 μm.

5. Particle mass distributions for all three consumables was spread over larger particles sizes and most of the mass was larger than the size considered to be in the harmful respirable range (> 0.1 μm).

6. The mass of particles in the ultrafine regime was very low, representing less than 2% of the total fume mass.

7. Varying heat input for the E6010 and E308-16 electrodes produced little change in number or mass distributions.

8. E7018 produced more particles in the finer regimes than E6010 and E308-16, though the highest measured concentration of particles was approximately 0.1 μm for both mild steels and 0.2 μm for the stainless steel.

Acknowledgments

The authors would like to thank Matt Gonser of the Welding & Joining Metallurgy Group at The Ohio State University for his valuable assistance in fume collection and analysis. Also thanks to Troy Paskell of WeldQC for help with equipment setup and testing. Funding for this project was provided by D&L Welding Fume Analysis LLC, representing a consortium of past and current consumable manufacturers.

References

1. Ashburner, L. 1989. Some hazards of welding fume. *Joining and Materials* 2(3): 118, 119.

2. NIOSH. 1988. *Criteria for a recommended standard – welding, brazing, and thermal cutting*. NIOSH document no. 88-110. Cincinnati, Ohio.

3. Pekkari, B. 2000. Growing concerns about health, safety and environment in welding. *Welding in the World* 44(5): 101 to 116.

4. Evans, R. M., Flanigan, L. J., Howden, D. G., Lee, K. W., Luce, R. G., Martin, D. C., Pattee, H. E., and Robinson, R. E. 1979. *Fumes and Gases in the Welding Environment,* Batelle-Columbus. Miami, Fla.: American Welding Society.

5. Fasiska, E. J., Wagenblast, H. W., and Nasta, M. 1983. *Characterization of Arc Welding Fume*. Miami, Fla.: American Welding Society.

6. Voitkevich, V. 1995. *Welding Fumes: Formation, Properties and Biological Effects*. Cambridge, England: Abington Publishing.

7. Jenkins, N. T. 2003. Chemistry of airborne particles from metallurgical processing. PhD dissertation, Massachusetts Institute of Technology, Cambridge, Mass.

8. Stephenson, D., Seshadri, G., and Veranth, J. M. 2003. Workplace exposure to submicron particle mass and number concentrations from manual arc welding of carbon steel. *American Industrial Hygiene Association Journal* 64: 516 to 521.

9. Zimmer, A. T., and Biswas, P. 2001. Characterization of aerosols resulting from arc welding processes. *Journal of Aerosol Science* 32: 993 to 1008.

10. Zimmer, A. T., Baron, P., and Biswas, P. 2002. The influence of operating parameters on number-weighted aerosol size distribution generated from a gas metal arc welding process. *Journal of Aerosol Science* 33: 519 to 531.

11. Reist, P. C. 1984. *Introduction to Aerosol Science*. New York, N.Y.: Macmillan Publishing.

12. Kelly, W. P., and McMurray, P. H. 1992. Measurement of particle density by inertial classification of differential mobility analyzer-generated monodisperse aerosol. *Aerosol Science and Technology* 17: 199 to 212.

13. Kutz, S., and Schmidt-Ott, A. 1990. Use of a low pressure impactor for fractal analysis of submicron particles. *J. Aerosol Science* 21(Suppl. 1): S47 to S50.

14. Gray, C. N., Hewitt, P. J., and Dare, P. R. M. 1982. New approach would help control fumes at source part two: MIG fumes. *Welding and Metal Fabrication* 51(1): 52 to 55.

15. Hinds, W. 1999. *Aerosol Technology: Properties, Behavior, and Measurement of Airborne Particles*, 2d ed. New York: Wiley-Interscience.

16. Seinfeld, J. H., and Pandis, S. 1998. *Atmospheric Chemistry and Physics*. New York: John Wiley & Sons Inc.

17. Ehrman, S. H., Friedlander, S. K., and Zachariaht, M. R. 1998. Characteristics of SiO_2/ TiO_2 nanocomposite particles formed in a premixed flat flame. *Journal of Aerosol Science* 29(5,6): 687 to 706.

18. Antonini, J. M., Krishna Murthy, G. G., Rogers, R. A., Albert, R., Eagar, T. W., Ulrich, G. D., and Brain, J. D. 1998. How welding fumes affect the welder. *Welding Journal* 77(10): 55 to 59.

19. American Welding Society. 1999. F1.2:1999, *Laboratory Method for Measuring Fume Generation Rates and Total Fume Emission of Welding and Allied Processes*. Miami, Fla.: AWS.

20. Keskinen, J., Pietarinen, K., and Lehtimäki, M. 1992. Electrical low pressure impactor. *J. Aerosol Science* 23(4): 353 to 360.

21. Speight, F. Y., and Campbell, H. C., eds. 1979. *Fumes and Gases in the Welding Environment*. Miami, Fla.: American Welding Society.

22. Sowards, J. W., Lippold, J. C., Dickinson, D. W., and Ramirez, A. J. 2008. Characterization procedure for the analysis of arc welding fume. *Welding Journal* 87(3): 76-s to 83-s.

23. Li, W., Perzl, M., Heyder, J., Langer, R., Brain, J. D., Englmeier, K. H., Niven, R. W., and Edwards, D. A. 1996. Aerodynamics and aerosol particle deaggregation phenomena in model oral-pharyngeal cavities. *Journal of Aerosol Science* 27(8): 1269 to 1286.

24. Dekati, Ltd. 2003. ELPI Users Manual. Tampere, Finland, Dekati Ltd.